Title

Dual-Mode HDAC Prodrug for Covalent Modification and Subsequent Inhibitor Release.

Journal

Journal of medicinal chemistry, 58(11)

ISSN

0022-2623

Authors

Daniel, Kevin B
Sullivan, Eric D
Chen, Yao
et al.

Publication Date

2015-06-01

DOI

10.1021/acs.jmedchem.5b00539

Peer reviewed

Journal of Medicinal Chemistry

Article

pubs.acs.org/jmc

Dual-Mode HDAC Prodrug for Covalent Modification and Subsequent Inhibitor Release

Kevin B. Daniel,[†] Eric D. Sullivan,[‡] Yao Chen,[†] Joshua C. Chan,[†] Patricia A. Jennings,[†] Carol A. Fierke,*[,‡,§,∥] and Seth M. Cohen*[,†]

[†]Department of Chemistry and Biochemistry, University of California, San Diego, La Jolla, California 92093, United States

[‡]Interdepartmental Program in Chemical Biology, [§]Department of Biological Chemistry, and [∥]Department of Chemistry, University of Michigan, Ann Arbor, Michigan 48109, United States

Supporting Information

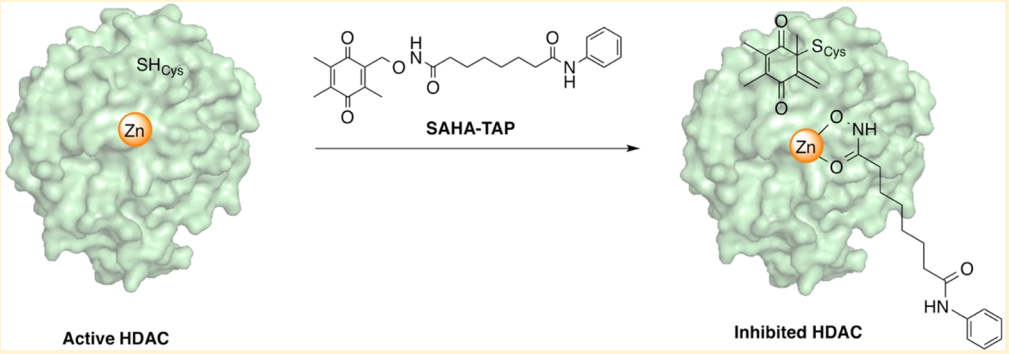

ABSTRACT: Histone deacetylase inhibitors (HDACi) target abnormal epigenetic states associated with a variety of pathologies, including cancer. Here, the development of a prodrug of the canonical broad-spectrum HDACi suberoylanilide hydroxamic acid (SAHA) is described. Although hydroxamic acids are utilized universally in the development of metalloenzyme inhibitors, they are considered to be poor pharmacophores with reduced activity in vivo. We developed a prodrug of SAHA by appending a promoiety, sensitive to thiols, to the hydroxamic acid warhead (termed SAHA-TAP). After incubation of SAHA-TAP with an HDAC, the thiol of a conserved HDAC cysteine residue becomes covalently tagged with the promoiety, initiating a cascade reaction that leads to the release of SAHA. Mass spectrometry and enzyme kinetics experiments validate that the cysteine residue is covalently appended with the TAP promoiety. SAHA-TAP demonstrates cytotoxicity activity against various cancer cell lines. This strategy represents an original prodrug design with a dual mode of action for HDAC inhibition.

INTRODUCTION

Transcription is a tightly regulated biological process that is the first step in gene expression.[1−3] In eukaryotic cells, sequence-specific DNA binding factors control the flow of genetic information from DNA to RNA, thereby regulating transcription. In cells, DNA is tightly compacted into chromatin, a highly organized and dynamic complex between DNA and proteins. When gene transcription is activated, the DNA is made accessible to transcription factors via nucleosome modification.[1,2] The local architecture of chromatin, which is influenced by post-translational modifications of histones, can regulate gene expression. These modifications include methylation, phosphorylation, and acetylation of core histones. Histone acetylation occurs at the ϵ-amino groups of conserved lysine residues near the N-termini. Acetylation levels of core histones are a result of the balance between histone acetyltransferases (HATs) and histone deacetylases (HDACs).[1−4] Increased levels of histone acetylation are generally associated with transcriptional activity, whereas decreased levels of histone acetylation are associated with repression of transcription. Additionally, acetylation of specific lysines on histone tails facilitates the recruitment of bromodomain-containing chromatin remodeling factors.[5,6] Furthermore, acetylated lysines have been observed in many cellular proteins, indicating that HATs and HDACs do not function solely to modify histones.[7]

Histone deacetylase inhibitors (HDACi) have been developed as a class of therapeutic agents intended to target aberrant epigenetic states associated with a variety of pathologies, most notably cancer.[8] Recent findings have shown that the relief of oncogenic transcriptional repressors by HDACi can lead to cell cycle arrest and apoptosis.[1−4] This is because many cancers have evolved such that pro-apoptotic pathways are transcriptionally repressed via histone deacetylation. HDACi prevent deacetylation of the lysine residues of the histone tails, which, in turn, leads to transcriptional activation, gene expression, and cell death.[1,8]

Received: April 6, 2015
Published: May 14, 2015

DOI: 10.1021/acs.jmedchem.5b00539
J. Med. Chem. 2015, 58, 4812−4821

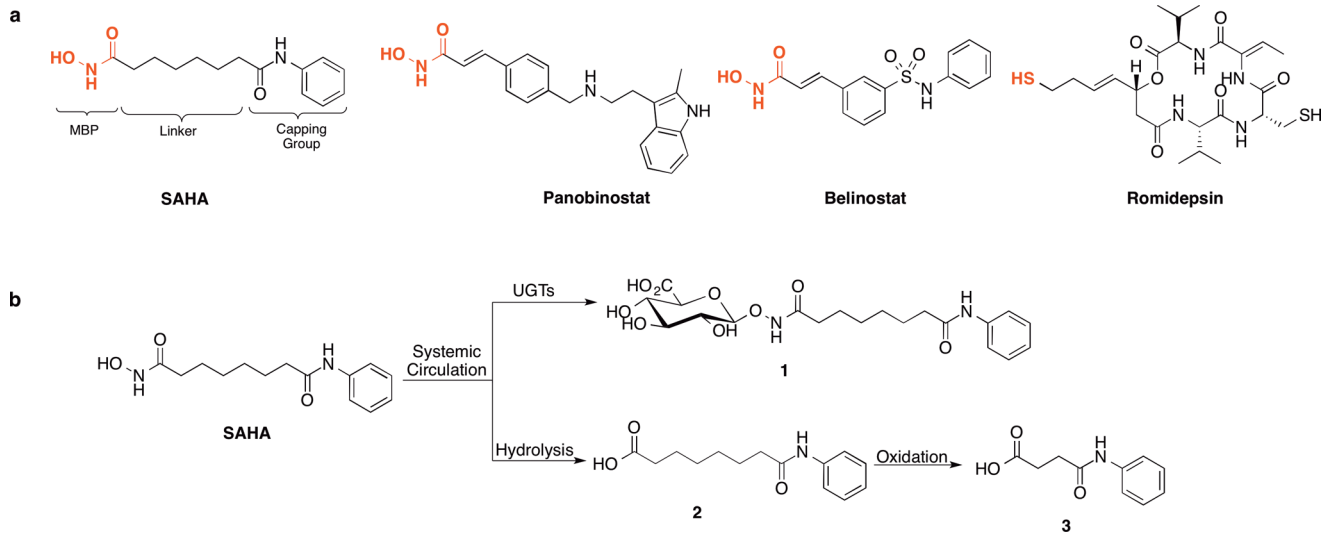

Figure 1. FDA-approved HDAC inhibitors. (a) The hydroxamic acid and sulfhydryl MBP donor atoms of SAHA, Panobinostat, Belinostat, and Romidepsin are shown in red. (b) Metabolism of SAHA. Upon systemic circulation, UGT enzymes localized in the liver can convert SAHA to a SAHA β-D-glucuronide (**1**), rendering the drug inactive. A different pathway involves initial hydrolysis of SAHA to the corresponding carboxylic acid (**2**), followed by oxidation to **3**.

The development of HDACi has been ongoing, and >10 candidates have progressed to clinical trials.[3] HDACi can be subdivided into structural classes including hydroxamic acids, cyclic peptides, aliphatic acids, and benzamides.[9] The HDACi Vorinostat (suberoylanilide hydroxamic acid, SAHA) received approval by the United States Food and Drug Administration (FDA) in 2006 for the treatment of cutaneous T-cell lymphoma (CTCL).[10] Crystallization of SAHA with HDAC8 supported a model involving the linkage of a metal-binding pharmacophore (MBP) to a capping group designed to form favorable interactions with amino acid residues at the entrance to the active site tunnel (Figure 1a).[11] Three other HDACi have been approved by the FDA, including Panobinostat and Belinostat, both broad-spectrum, hydroxamate-based HDACi for the treatment of multiple myeloma or relapsed/refractory peripheral T-cell lymphoma, respectively (Figure 1a).[12,13] Romidepsin (FK228), a cyclic peptide HDACi that uses a thiol group to coordinate the active site metal ion, is approved for CTCL treatment (Figure 1a).[10]

SAHA, Romidepsin, and Panobinostat act to inhibit most isoforms of the metal-dependent HDAC family and are regarded as broad-spectrum HDAC inhibitors. Despite promising clinical results for HDACi, these drugs have not been effective in clinical trials involving solid tumors. In fact, these FDA-approved drugs have been associated with the onset of serious side effects, including fatigue, gastrointestinal issues (diarrhea, nausea, vomiting), and hematologic complications (thrombocytopenia, anemia, neutropenia).[8,10] Both SAHA and Romidepsin have also been associated with cardiotoxicity.[8] Clinical studies in humans determined the major metabolic pathways of SAHA degradation involve glucoronidation by UDP-glucoronosyltransferases (UGTs) to generate inactive **1** (Figure 1b). Alternatively, hydrolysis of SAHA to the carboxylic acid analogue (**2**) followed by β-oxidation generates the inactive metabolite 4-anilino-4-oxobutanoic acid (**3**, Figure 1b).[10,14] Clinical studies determined that the mean steady-state serum exposures of **1** and **2** were 4- and 13-fold higher than SAHA, respectively. Additionally, the apparent $t_{1/2}$ of SAHA in human serum was ~1.5 h for patients receiving single doses of 400 mg of SAHA.[8,10,14] The poor pharmacokinetic (PK) properties of SAHA are similar for other hydroxamic acid-based compounds and involve chemical instability and rapid elimination.[8,15] In fact, the FDA has approved SAHA for CTCL only in patients with persistent or recurrent disease who have already followed two systemic therapies.[8] Similarly, the FDA has only approved Romidepsin for CTCL treatment in patients who have received at least one prior systemic therapy, and Panobinostat is administered only after two prior standard therapies have failed.[16] The onset of these deleterious side effects is proposed to originate, in part, from the lack of selectivity of these drugs for a specific HDAC isozyme.[8]

Chemically modified versions of active drugs have been developed in an effort to overcome barriers to drug formulation and delivery. The modified, latent version of the drug, termed the prodrug, undergoes a transformation in the presence of a desired chemical or enzymatic stimulus in vivo to generate the active agent.[17,18] The chemical group appended to the active drug rendering it inactive is termed the promoiety. Only a handful of reports have investigated HDAC prodrugs, with most studies focused on developing acyl derivatives of SAHA or similar hydroxamic acid-based HDACi to enhance cell permeability and hydrolytic stability.[19] As expected, these prodrugs showed little activity as HDAC inhibitors, and biochemical assays suggest that the acylated prodrugs are more cell-permeable than the hydroxamic acid parent drugs. A similar report investigated a carbamate prodrug concept for hydroxamate HDACi (including SAHA) to improve drug-like properties, including cellular permeability.[20] However, both of these strategies rely on hydrolysis in vivo to release the active drug and do not improve drug–target specificity for selected disease states or sites of disease.

Initially, we sought to develop new HDAC inhibitor prodrugs (proinhibitors) that become activated in the presence of thiols such as glutathione in its reduced form (GSH), which is frequently more abundant at the site of disease (e.g., cancer).[21] Previously, Huang and co-workers reported the development of a long-wavelength fluorescent probe involving a quinone-methide reaction that can detect physiologically

DOI: 10.1021/acs.jmedchem.5b00539
J. Med. Chem. 2015, 58, 4812–4821

relevant thiols including GSH.[22] Although the quinone promoiety functions as an electrophilic Michael acceptor, it was determined that other biologically relevant nucleophiles, including serine and lysine, were unreactive with this functionality. Our prodrug approach considered the covalent appendage of this quinone promoiety to the hydroxamate of an HDACi, since the alkylation of hydroxamates has been shown to be effective in improving PK properties including hydrolytic stability, cellular permeability, and glucoronidation.[19,23,24]

As described below, even in the absence of nucleophilic thiols, we observed activation of our prodrug (SAHA-TAP); sequence homology analysis revealed that a single cysteine (Cys) residue is conserved in all metal-dependent HDAC isoforms, which we found was reactive with our prodrug (Supporting Information, Figure S1).[25] The crystal structure of HDAC8 complexed with SAHA reveals that the conserved Cys (Cys153 for HDAC8) is located in the catalytic active site pocket ~5.6 Å away from the hydroxamic acid moiety of SAHA (Figure 2). Thus, we have concluded that our prodrug is

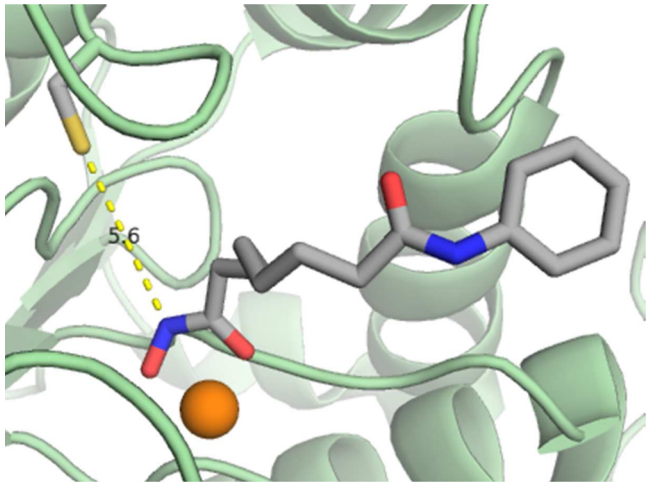

Figure 2. Protein crystal structure of HDAC8 complexed with SAHA. The distance between the sulfhydryl moiety of Cys153 and the nitrogen atom of the MBP of SAHA was determined to be 5.6 Å. SAHA and Cys153 are shown as sticks in color code (carbon, gray; nitrogen, blue; oxygen, red; sulfur, yellow), and the Zn^{2+} ion is shown as an orange sphere (PDB: 1T69).

cleaved by the sulfhydryl moiety of the conserved Cys of HDAC, leading to drug activation and a dual mode of inhibition: covalent modification of the conserved Cys leading to the formation of an inactive, covalently modified enzyme and release of the competitive inhibitor SAHA.

RESULTS AND DISCUSSION

Development of a Unique HDACi Prodrug. SAHA was chosen as the drug of interest because it is FDA-approved for the treatment of CTCL and has been well-studied. A prodrug of SAHA containing a quinone-based, thiol-sensitive promoiety was designed, termed SAHA-TAP (TAP, thiol activated prodrug) (Figure 3). To develop SAHA-TAP, the promoiety was first synthesized using a modified literature procedure.[22] The promoiety was appended to SAHA under basic conditions to generate SAHA-TAP. The activation of SAHA-TAP by reaction with GSH is summarized in Figure 3a. A control compound, SAHA-OBn, was synthesized in a similar manner. This compound contains a benzyl moiety appended to SAHA via the *N*-hydroxyl functionality. SAHA-OBn was designed to have a similar structure as that of SAHA-TAP but to be unreactive toward nucleophilic thiols.

Assessment of SAHA-TAP Reactivity with GSH. To evaluate the reactivity of SAHA-TAP and SAHA-OBn with nucelophilic thiols, analytical HPLC was utilized under simulated physiological conditions (50 mM HEPES, pH 7.4). SAHA-TAP was treated with GSH (2 mM, 2 equiv) to confirm that the prodrug is indeed reactive with thiols. After incubation of SAHA-TAP with GSH, three distinct peaks were apparent in the HPLC chromatogram (Figure 3b). Liquid chromatography−mass spectrometry (LC-MS) confirms that the identity of the first peak (t_R = 10.5 min) is the quinone-methide side product, the second peak is SAHA (t_R = 10.7 min), and the third peak is unreacted SAHA-TAP (t_R = 14.7 min). Treatment of SAHA-OBn with GSH under the same conditions resulted in no change in the HPLC chromatogram, indicative of the expected lack of reactivity (Figure 3c). Having shown that SAHA-TAP reacts rapidly with GSH, the aqueous stability of SAHA-TAP was evaluated under simulated physiological conditions (50 mM HEPES, pH 7.4). An HPLC chromatogram was obtained immediately after preparation in aqueous buffer, and a second trace was collected after incubation at 37 °C for 24 h. SAHA-TAP was determined to be >97% stable to hydrolysis in the absence of thiols (Figure S2).

HDAC Inhibition by SAHA-TAP. To determine the efficacy of the SAHA-TAP prodrug strategy, the ability of SAHA-TAP and SAHA-OBn to inhibit HDAC-1, -2, -3, -6, and -8 was evaluated using an optimized homogeneous fluorescence-based assay (BPS Bioscience). Surprisingly, even in the absence of exogenous thiols, SAHA-TAP was an effective inhibitor of all HDACs tested, with an apparent IC_{50} value that is slightly less potent (2- to 50-fold) than that of the parent inhibitor, SAHA (Table S1). This result was unexpected because the metal-binding ability of the hydroxamic acid MBP of SAHA-TAP is blocked by the promoiety, which should render the drug nearly inactive. Recent studies indicate that the metal-free form of HDAC8 has a low affinity for SAHA analogues, further demonstrating the importance of metal binding for HDAC inhibition.[26] To determine if a component of the biochemical assay resulted in SAHA-TAP activation, analytical HPLC was utilized. SAHA-TAP was incubated with either BSA (5 mg/mL) or trypsin (5 mg/mL) at 37 °C for 2 h; however, SAHA-TAP was found to be >95% stable in the presence of either of these assay components (data not shown).

Because SAHA-TAP is a larger molecule than SAHA and the metal-binding hydroxamate group is blocked, it is feasible that the promoiety may be positioned very close to Cys153 when bound to HDAC8. This positioning could be ideal for nucleophilic attack by the sulfhydryl moiety, leading to covalent modification and SAHA release. We hypothesized that the Cys153 residue of HDAC8 reacts with bound SAHA-TAP, resulting in a covalent modification of the protein and subsequent release of SAHA, a competitive inhibitor (Figure S3). It is important to note that there are many other Cys residues in the metal-dependent HDAC isoforms (e.g., 10 Cys residues in HDAC8), and activation of SAHA-TAP by these residues may also be responsible, in part, for the release of SAHA that we observe (vide supra).

Mass Spectrometry Analysis. To investigate whether the active site Cys153 is covalently modified by the SAHA-TAP promoiety, mass spectrometry (MS) techniques were utilized. Digestion of wild-type (WT) HDAC8 with trypsin yields an 18

DOI: 10.1021/acs.jmedchem.5b00539
J. Med. Chem. 2015, 58, 4812−4821

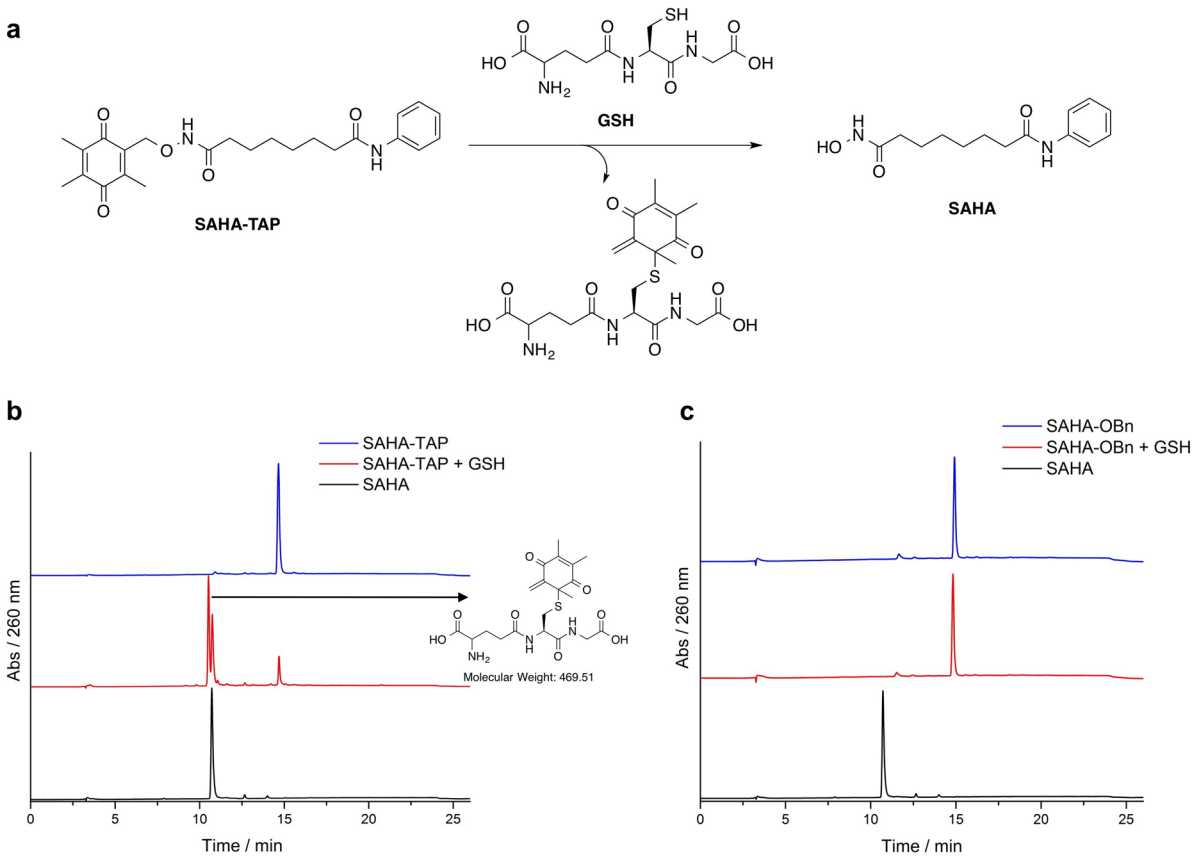

Figure 3. (a) Activation of SAHA-TAP by GSH. In the presence of GSH, the sulfhydryl moiety can attack the electrophilic quinone moiety. Subsequent rearrangement releases SAHA along with a quinone-methide adduct. (b) HPLC trace of SAHA (black), SAHA-TAP (blue), and SAHA-TAP after treatment with GSH (2 mM, 2 equiv) for 2 h at 37 °C (red). Retention times are 10.7 min for SAHA, 14.7 min for SAHA-TAP, and 10.5 min for the quinone-methide GSH adduct generated from the reaction. (c) HPLC trace of SAHA (black), SAHA-OBn (blue), and SAHA-OBn after incubation in HEPES (50 mM, pH 7.4) for 24 h at 37 °C (red). Retention times are 10.7 min for SAHA and 14.9 min for SAHA-OBn.

amino acid peptide containing Cys153, which can be used to monitor the modification via mass spectrometry (Figure 4a). If a covalent modification occurs at this position after treatment of WT HDAC8 with SAHA-TAP, then the expected MS ion for this peptide fragment will be different from the unmodified parent ion.

HDAC8 (WT, with or without incubation with a 12-fold excess of SAHA-TAP for 60 min at 37 °C) was digested with trypsin, and the resulting peptides were analyzed by LC-MS. The expected parent ion for the WT HDAC8 Cys153 peptide was consistent with a peak at t_R = 84.5 min (Figure 4b). Similarly, a peak at t_R = 88.5 min corresponds to the expected parent ion for the covalently modified Cys153 HDAC8 peptide after SAHA-TAP treatment (Figure 4c). To eliminate other digestion products that could account for this ion, further MS techniques were applied to verify that these ion peaks correspond to the peptide sequence of interest.

Tandem mass spectrometry (MS^2 or MS/MS) is routinely used in proteomics to characterize amino acid sequences of proteins, where peptides undergo further fragmentation to amino acid aggregates.[27] The fragmentation patterns observed in the MS/MS spectra of tryptic peptides for WT HDAC8 and SAHA-TAP treated HDAC8 were investigated to obtain additional insight into the possibility of covalent modification of Cys153. The expected monoisotopic masses for the *y* ion series in both WT HDAC8 and the SAHA-TAP treated sample are summarized in Table S2. The expected *y* fragment ions for both peptides align until Cys153 (y_{12}), where this ion and each subsequent ion have different masses. Indeed, the MS/MS fragmentation spectrum for the WT HDAC8 tryptic peptide (parent ion m/z = 1006.98, $[M + 2H]^{2+}$) shows many of the expected *y* ions (Figure S4). Similarly, the MS/MS fragmentation spectrum for the SAHA-TAP treated HDAC8 tryptic peptide (parent ion m/z = 1059.53 $[M + 2H]^{2+}$) shows many *y* ions, including the characteristic peak of m/z = 1511.82 (Figure S5). This peak is indicative of a covalent modification of m/z = 162.1 for the HDAC8 tryptic fragment at Cys153. These data prove that the covalent modification of Cys153 is occurring to form an adduct containing the SAHA-TAP promoiety, as shown in Figure S3.

MS analysis also indicated that Cys102, Cys244, and Cys314 could be modified by the TAP moiety from SAHA-TAP. Importantly, the peptides containing surface cysteines (Cys275 and Cys352) were not modified with TAP, suggesting that activation is not nonspecific. Nonetheless, the hypothesized mechanism of activation involving a covalent modification of Cys residues in HDAC8, including Cys153, was observed, which can aid in explaining the inhibition of HDACs by SAHA-TAP even in the absence of exogenous nucleophilic thiols, as observed in the in vitro assays.

In Vitro Time Dependence of SAHA-TAP HDAC Inhibition. With the MS data in hand confirming covalent modification of Cys residues in HDAC8, we sought to investigate the kinetics of inhibition of HDAC8 by SAHA-

DOI: 10.1021/acs.jmedchem.5b00539
J. Med. Chem. 2015, 58, 4812−4821

a

DEASGF**C**YLNDAVLGILR

Fragment Type	Expected Ion $[M+2H]^{2+}$
WT HDAC8	1006.98 *m/z*
SAHA-TAP treated HDAC8	1060.16 *m/z*

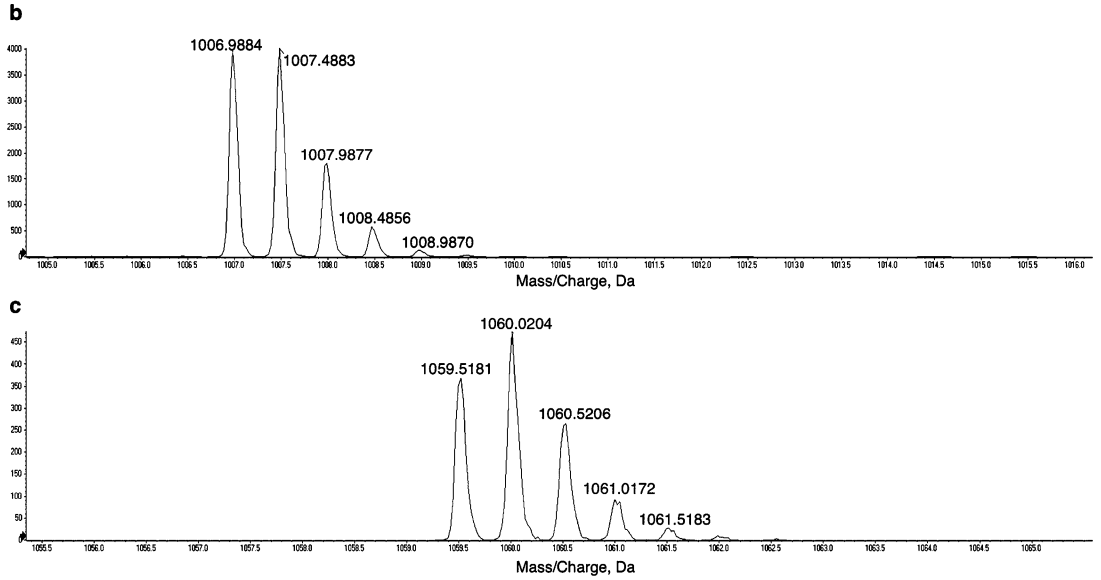

Figure 4. HDAC8 tryptic fragment MS data. (a) Expected HDAC8 Cys153 peptide upon digestion with trypsin (Cys153 in bold). The expected MS ion for the WT protein is shown along with the expected ion for the peptide including the covalent addition of the TAP promoiety on Cys153. (b) The tryptic fragment of WT HDAC8 (t_R = 84.5 min) is consistent with the expected $[M + 2H]^{2+}$ ion. (c) After treatment of HDAC8 with SAHA-TAP (12 equiv) and digestion with trypsin, a peak aligning with the expected $[M + 2H]^{2+}$ ion is observed (t_R = 88.5 min).

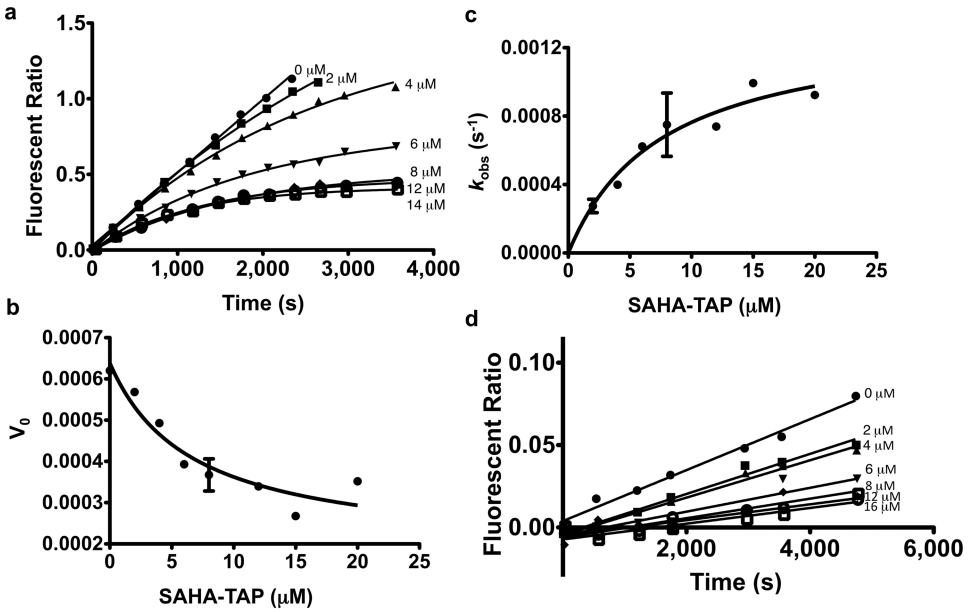

Figure 5. Time dependence of HDAC8 inhibition. (a) WT HDAC8 (0.5 μM) progress curves at varying concentrations (0–20 μM) of SAHA-TAP. Dependence of both the (b) initial rate, v_0, and (c) k_{obs} on the concentration of SAHA-TAP. (d) C153A HDAC8 (2 μM) progress curves at varying concentrations (0–20 μM) of SAHA-TAP.

TAP using the Fluor-de-Lys activity assay (Enzo Life Sciences). A previous study determined that the catalytic activity and thus inhibition of HDAC8 is dependent on the identity of the active site metal ion (e.g., Co^{2+}, Fe^{2+}, Zn^{2+}, and Ni^{2+}).[28] To obtain the most accurate results, apo-HDAC8 (human, recombinant) was initially prepared before the addition of Zn^{2+} in a 1:1 stoichiometry. An initial test of HDAC8 inhibition by preincubation of the enzyme with SAHA-TAP demonstrated that activity loss occurred within the first 0.5 h (data not shown). To determine the kinetics for the time-dependent

DOI: 10.1021/acs.jmedchem.5b00539
J. Med. Chem. 2015, 58, 4812–4821

inhibition by SAHA-TAP, HDAC8 progress curves were measured through a range of inhibitor concentrations (Figure 5a). For these reactions, the Fluor-de-Lys HDAC8 substrate (150 μM) and SAHA-TAP (0−20 μM) were added to each assay prior to initiating the reactions with WT HDAC8 (0.5 μM). Over a time course, aliquots of the reactions were stopped by dilution into a solution of trichostatin A and trypsin, and product formation was analyzed from the resulting change in fluorescence. Analysis of the HDAC8 progress curves in the presence of increasing concentrations of SAHA-TAP demonstrates a nonlinear formation of product with respect to time. Equation 1, which describes the time-dependent decrease in initial velocity under steady-state turnover conditions,[29,30] was fit to the progress curves

$$P = \frac{(v_s t) + (v_0 - v_s) \times [1 - \exp(-k_{obs} t)]}{k_{obs} + C} \quad (1)$$

where P represents production formation, v_s and v_0 represent final and initial velocities, respectively, t is time, C is the initial fluorescent ratio, and k_{obs} is the rate constant describing the transition from the initial velocity to the final steady-state velocity, reflecting the time-dependent enzyme inactivation.

This fit reveals that both the initial velocity and the rate constant for inactivation, k_{obs}, have a hyperbolic dependence on the concentration of SAHA-TAP (Figures 5b,c). The initial velocity decreases with an apparent $K_i = 7 \pm 4$ μM, and the rate constant for inactivation increases with a $K_{1/2} = 8 \pm 2$ μM to a maximal rate constant of 0.0013 s^{-1} at saturating SAHA-TAP. This type of inhibition is characteristic of a two-step mechanism (Scheme 1) in which a rapid reversible step, such as binding of SAHA-TAP to HDAC8, is followed by a time-dependent step, consistent with irreversible inactivation.[29,30] These data demonstrate that the prodrug, SAHA-TAP, is capable of binding to and inhibiting HDAC8. The time-dependent decrease in activity is consistent with the MS data demonstrating the formation of a covalent enzyme adduct.

$$E + I \overset{K_i}{\rightleftharpoons} E{\cdot}I \xrightarrow{k_{obs}} E{-}I \quad \text{(Scheme 1)}$$

For comparison, progress curves for inhibition of HDAC8 with the competitive inhibitor SAHA and a negative control, SAHA-OBn, were evaluated. These assays were performed in the same manner as the SAHA-TAP progress curves, where substrate and inhibitor were added to the assay prior to the addition of HDAC8 to initiate the reaction. In contrast to the data with SAHA-TAP, these progress curves are linear with no observable curvature for all concentrations of SAHA (Figure S6a) and SAHA-OBn (Figure S6b). As expected, HDAC8 (0.5 μM) is inhibited >90% by SAHA in the concentration range tested (2−8 μM), which is in agreement with the 250 nM K_i reported for Zn^{2+}-HDAC8.[28] SAHA-OBn (2−10 μM) does not inhibit the activity of HDAC8. The lack of inhibition by SAHA-OBn is consistent with previous IC_{50} data (Table S1). Taken together, these data show that SAHA-TAP has a unique mode of inhibition for HDAC8 when compared to SAHA. This inhibitor functions both as a competitive inhibitor and as a time-dependent inactivator, in contrast to the linear, time-independent inhibition observed for SAHA.

To determine the role of Cys153 in the time-dependent inhibition of HDAC8, a Cys153Ala (C153A) HDAC8 mutant was prepared and purified. In vitro assays for the mutant were conducted under the same conditions used for WT HDAC8. Progress curves for these assays reveal dose-responsive inhibition with $K_i = 8 \pm 4$ μM for SAHA-TAP (Figures 5d and S7). Furthermore, these progress curves are linear for all concentrations of inhibitor, showing a loss of the time-dependent inhibition observed with WT HDAC8. This data suggests that SAHA-TAP, containing the same linker spacer and capping group as SAHA, can bind HDAC8 in a noncovalent manner, inhibiting the enzyme (Scheme 1). The linear progress curves also demonstrate that Cys153 is important for the time-dependent inactivation, eliminating an alternate explanation that the time-dependent inhibition is due to the slow formation of SAHA from SAHA-TAP. Progress curves with C153A HDAC8 measured with SAHA and SAHA-OBn data reveal that the HDAC8 mutant remains susceptible to inhibition by SAHA and not SAHA-OBn (Figure S8).

Collectively, these data indicate both that SAHA-TAP binds noncovalently to HDAC8 to inhibit the activity and that the time-dependence mainly reflects the reaction of SAHA-TAP with Cys153. Although the MS data suggests that SAHA-TAP can react with other Cys residues in HDAC8, leading to SAHA release, C153A HDAC8 is not inactivated in a time-dependent manner, demonstrating the importance of this particular Cys in the mechanism of inhibition for the WT enzyme. The combination of the enzyme kinetics and MS data provides evidence that the inactivation of HDAC8 by SAHA-TAP involves two steps: noncovalent binding of SAHA-TAP to HDAC8 followed by covalent modification of Cys153.

Plasma Stability. As mentioned earlier, SAHA suffers from poor PK properties, including hydrolytic instability with $t_{1/2} \sim 1.5$ h. To determine the stability of SAHA-TAP in a biologically relevant model, human plasma stability studies were conducted as previously reported.[31] After incubating SAHA or SAHA-TAP in human plasma, aliquots were withdrawn at various time points (0, 15, 30, 60, and 120 min), quenched with acetonitrile, filtered, and evaluated via analytical HPLC. The percent parent compound remaining was determined by integrating the area under the curve and comparing this number with the initial sample of parent compound at an incubation time of 0 min. Approximately 72% of SAHA-TAP remained after 1 h incubation at 37 °C, whereas only ∼60% of SAHA remained under identical conditions. Only ∼50% of either parent compound remained after a 2 h incubation at 37 °C (Figure 6a). After 2 h incubation at 37 °C, the HPLC trace of SAHA-TAP showed that the major degradation peak (∼23%) corresponds to SAHA, with ∼52% SAHA-TAP remaining and ∼25% other products. This suggests that hydrolysis of SAHA-TAP to SAHA is a major component of the degradation process in human plasma (Figure S9). For comparison, after a 2 h incubation in human plasma under identical conditions, the HPLC chromatogram for SAHA shows the emergence of a series of new unidentifiable peaks (∼45%), with ∼55% SAHA remaining (Figure S9). Even though SAHA-TAP gradually degrades over this 2 h period, it is relatively slow and results in the release of the active drug SAHA. Efforts to identify other product peaks via LC-MS were inconclusive. Overall, this study indicates that SAHA-TAP has a moderately improved stability profile than SAHA in human plasma.

Cell Proliferation Studies. With the kinetics of activation and plasma stability of SAHA-TAP elucidated, we then studied the effect of SAHA-TAP on the proliferation of a variety of cell lines. Because SAHA is FDA-approved for CTCL, we selected HH (CTCL) and Jurkat (T-cell leukemia) cell lines for analysis. The viability of NIH/3T3 (mouse embryo fibroblast) was also tested to determine the toxicity of each compound for a

DOI: 10.1021/acs.jmedchem.5b00539
J. Med. Chem. 2015, 58, 4812−4821

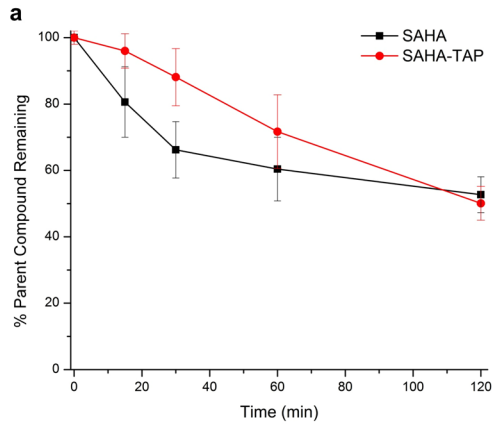

b

Compound	HH	Jurkat	NIH/3T3
SAHA	1.03±0.21 μM	1.66±0.14 μM	4.80±0.99 μM
SAHA-TAP	3.38±0.30 μM	6.05±0.14 μM	9.37±1.21 μM
SAHA-OBn	NI	NI	NI

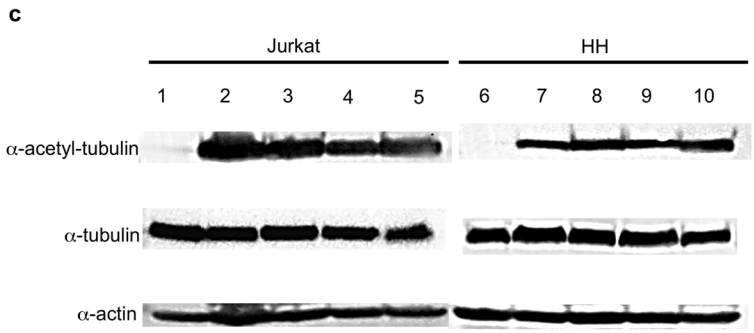

Figure 6. (a) Plasma stability for SAHA (red circles) and SAHA-TAP (black squares) over time (mean ± SD). (b) Cellular EC_{50} values (μM) obtained from the MTS cell proliferation assay. NI, no inhibition at 50 μM. (c) Western blot analysis of tubulin acetylation for Jurkat (lanes 1−5) and HH (lanes 6−10) cells. Lane 1, control (no treatment); lane 2, SAHA (1.5 μM); lane 3, SAHA (20 μM); lane 4, SAHA-TAP (6 μM); lane 5, SAHA-TAP (20 μM); lane 6, control (no treatment); lane 7, SAHA (1.5 μM); lane 8, SAHA (20 μM); lane 9, SAHA-TAP (6 μM); lane 10, SAHA-TAP (20 μM).

noncancer cell line. The EC_{50} values of SAHA, SAHA-TAP, and SAHA-OBn are shown in Figure 6b for each cell line. The observed EC_{50} values of SAHA for HH and for Jurkat cell lines were 1.03 ± 0.21 μM and 1.66 ± 0.14 μM, respectively, consistent with previously reported data.[32,33] SAHA-TAP is ∼3−4-fold less potent than SAHA, but it is still an active compound, with calculated EC_{50} values of 3.38 ± 0.30 μM and 6.05 ± 0.14 μM for HH and Jurkat cells, respectively. This difference in potency may be attributed to the alkylated Cys affecting the binding of SAHA to HDAC8; further structural studies are needed to confirm this hypothesis. Interestingly, SAHA also is toxic for NIH/3T3 cell lines, with a calculated EC_{50} of 4.80 ± 0.99 μM. Other studies also report cytotoxicity of healthy kidney cells (Vero) after treatment with SAHA (EC_{50} = 5.20 ± 0.96 μM).[28] Unfortunately, cell proliferation studies indicate that SAHA-TAP is also slightly toxic for NIH/3T3 cells with an apparent EC_{50} value of 9.37 ± 1.21 μM. As expected, cell proliferation is unaffected by the addition of SAHA-OBn for all cells studied.

Intracellular Target Validation. With the cell proliferation data in hand for both Jurkat and HH cells, we sought to validate the intracellular target of SAHA-TAP using western blotting techniques. Broad-spectrum HDACi are known to increase the steady-state accumulation of tubulin, an endogenous HDAC substrate and a common marker for intracellular HDAC6 activity.[34,35] For these experiments, SAHA was used as a positive control, since it has been shown to dramatically increase tubulin acetylation in a variety of cells.[33,36] Indeed, we observed that SAHA-TAP increased tubulin acetylation in both Jurkat and HH cells without disturbing actin levels (Figure 6c), suggesting that the antiproliferative mechanism of action for SAHA-TAP, like SAHA, involves nonspecific HDAC inhibition.

CONCLUSIONS

A thiol-sensitive prodrug of the FDA-approved HDACi SAHA has been developed that displays a time-dependent inhibition of HDAC8. SAHA-TAP functions as a dual-mode HDAC inhibitor with both a covalent modification and a noncovalent, conventional mode of action. SAHA-TAP is susceptible to nucleophilic attack by Cys residues on the target HDAC, particularly the conserved Cys153 residue in the catalytic domain of HDAC8. These Cys residues are covalently modified with the promoiety, inactivating the enzyme, followed by the release of the competitive inhibitor SAHA. Proteomic MS confirms that this modification occurs at Cys153, and the kinetics of inhibition show unambiguous time-dependent inhibition of HDAC8 by SAHA-TAP, indicative of a covalent modification with release of SAHA. The HDAC8 C153A mutant retains the noncovalent mode of inhibition by SAHA-TAP (Scheme 1), whereas the time-dependent mode of inhibition disappears. This result demonstrates the importance of the active site Cys in the inactivation of HDAC8 by SAHA-TAP. The stability of SAHA-TAP in human plasma is slightly improved, with slow conversion to SAHA observed. In contrast, SAHA is rapidly degraded to several products under identical conditions, consistent with previous literature studies. Finally, cellular proliferation studies show a clear dose−response relationship with SAHA-TAP for two distinct cancer cell lines, with only moderately inferior EC_{50} values compared to SAHA; immunoblotting confirms that the antiproliferative

DOI: 10.1021/acs.jmedchem.5b00539
J. Med. Chem. 2015, 58, 4812−4821

mechanism of action of SAHA-TAP involves HDAC inhibition. To the best of our knowledge, SAHA-TAP is the first dual-mode HDAC proinhibitor that exploits the modification of endogenous, conserved Cys residues, namely, the catalytic site Cys153 residue in HDAC8, to generate a covalent adduct in addition to releasing a competitive inhibitor.

EXPERIMENTAL SECTION

Enzyme Inhibition Assays. HDAC-1, -2, -3, -6, and -8 activity was determined in vitro with an optimized homogeneous assay performed in a 384-well plate. Recombinant, full-length HDAC protein (BPS Biosciences) was incubated with fluorophore-conjugated substrate, MAZ1600 and MAZ1675, at [substrate] = K_m (MAZ1600; 11 μM for HDAC1, 18 μM for HDAC2, 9 μM for HDAC3, 4 μM for HDAC6; MAZ1675; 263 μM for HDAC8). Reactions were performed in assay buffer (50 mM HEPES, 100 mM KCl, 0.001% Tween-20, 0.05% BSA, pH 7.4, and additional 200 μM TCEP was added for HDAC6) and followed by fluorogenic release of 7-amino-4-methylcoumarin from substrate upon deacetylase and trypsin enzymatic activity. Flourescence measurements were obtained every 5 min using a multilabel plate reader and plate stacker (Envision; PerkinElmer). Each plate was analyzed by plate repeat, and the first derivative within the linear range was imported into analytical software (Spotfire DecisionSite). Replicate experimental data from incubations with inhibitor were normalized to DMSO controls ([DMSO] < 0.5%). IC_{50} values are determined by logistic regression with unconstrained maximum and minimum values.

Mass Spectrometry Experiments. Preparation. An aliquot of HDAC8 (1.7 μM) was incubated with SAHA-TAP (12 equiv, 20 μM) at 37 °C for 1 h. The protein was purified by SDS-PAGE followed by Coomassie staining prior to analysis.

In Gel Digest. The gel slices of interest were cut to 1 mm cubes and destained three times by first washing with 100 mM ammonium bicarbonate (100 μL) for 15 min followed by the addition of ACN (100 μL) for 15 min. The supernatant was collected, and samples were dried in a SpeedVac. The samples were then reduced by the addition of 100 μM ammonium bicarbonate/10 mM DTT (200 μL) and incubated at 56 °C for 30 min. The liquid was removed, and 100 mM ammonium bicarbonate/55 mM iodoacetamide (200 μL) was added to gel pieces and incubated at RT in the dark for 20 min. After the removal of the supernatant and one wash with 100 mM ammonium bicarbonate for 15 min, the same volume of ACN was added to dehydrate the gel pieces. The solution was then removed, and the samples were dried in a SpeedVac. For digestion, enough solution of ice-cold trypsin (0.01 μg/mL) in 50 mM ammonium bicarbonate was added to cover the gel pieces, which were then incubated on ice for 30 min. After complete rehydration, the excess trypsin solution was removed, replaced with fresh 50 mM ammonium bicarbonate, and incubated overnight at 37 °C. The peptides were extracted twice by the addition of 0.2% formic acid and 5% ACN (50 μL) and vortex mixing at RT for 30 min. The supernatant was removed and saved. A total of 50 μL of 50% ACN/0.2% formic acid was added to the sample, which was vortexed again at RT for 30 min. The supernatant was removed and combined with the supernatant from the first extraction. The combined extractions were analyzed directly by LC-MS.

LC-MS/MS. Trypsin-digested peptides were analyzed by HPLC coupled with tandem mass spectrometry (LC-MS/MS) using nanospray ionization. The nanospray ionization experiments were performed using a TripleTOF 5600 hybrid mass spectrometer (SCIEX) interfaced with nanoscale reversed-phase HPLC (Tempo) using a 10 cm × 100 μm i.d. glass capillary packed with 5 mm C18 Zorbax beads (Agilent Technologies). Peptides were eluted from the C18 column into the mass spectrometer using a linear gradient (5–60%) of ACN at a flow rate of 250 μL/min for 1 h. The buffers used to create the ACN gradient are buffer A (98% H_2O, 2% ACN, 0.2% formic acid, and 0.005% TFA) and buffer B (0.2% formic acid and 0.005% TFA in ACN). MS/MS data were acquired in a data-dependent manner in which the MS1 data was acquired for 250 ms at m/z of 400 to1250 Da and the MS/MS data was acquired from m/z of 50 to 2000 Da. Independent data acquisition (IDA) parameters were MS1-TOF 250 ms followed by 50 MS2 events of 25 ms each. The IDA criteria were as follows: over 200 counts threshold, charge state +2–4, with 4 s exclusion. Finally, the collected data were analyzed using MASCOT (Matrix Sciences).

Protein Expression and Purification. Recombinant human HDAC8 in a pET-20b-derived plasmid with an added C-terminal TEV protease cleavage site and His_6 tag (termed pHD)[28] was expressed and purified in *Escherichia coli* BL21(DE3) according to Gantt and co-workers,[28] with the following modification: elution from the nickel columns was performed using a linear gradient (10–250 mM imidazole). In the preparation of apo-enzyme, HDAC8 was dialyzed twice at 4 °C against 4 L of 25 mM MOPS, 1 mM EDTA, 5 mM KCl, 1 mM TCEP, pH 7.5, followed by four times against 2 L of 25 mM MOPS, 5 mM KCl, 1 mM TCEP, pH 7.5. All components were free of transition metals, and dialysis occurred in plasticware that had been washed with EDTA and rinsed with Milli-Q ddH_2O. Apo-enzyme was stored at −80 °C in the same metal-free buffer. The Cys153Ala HDAC8 mutant was constructed in a pHD4 TEV-His plasmid, using the QuikChange site-directed mutagenesis protocol and kit, and the mutation was confirmed by the UM DNA sequencing facility. This construct was expressed and purified in the same manner as wild-type enzyme.

HDAC8 Time-Course Inhibition Experiments. Recombinant WT or C153A mutant human HDAC8 was reconstituted for 1 h on ice at a 1:1 stoichiometry (at 10 μM) with Zn^{2+} in 1× HDAC assay buffer (25 mM HEPES, 3 mM KCl, 137 mM NaCl, pH 8.0). The 5 and 50 mM SAHA-TAP, SAHA-OBn, and SAHA stocks were serially diluted into decreasing concentrations of DMSO to maintain solubility of the compounds. Reaction mixtures of 1× HDAC assay buffer, 150 μM Fluor-de-Lys peptide substrate (R–H–K(Ac)–K(Ac)–fluorophore) (Enzo Life Sciences), and various concentrations of inhibitors (SAHA-TAP, SAHA-OBn, or SAHA) were prepared and allowed to equilibrate at 30 °C. The final DMSO content was <1%. Assays were initiated by addition of wild-type (0.5 μM) or Cys153Ala mutant (2 μM) HDAC8. At various time points, a reaction aliquot (5 μL) was diluted into a Fluor-de-Lys quench solution (45 μL) containing trypsin and trichostatin A (TSA). Assays were read in 96-well plates (Corning 3686) using a PolarStar fluorescent plate reader. The fluorescence corresponding to product formation (λ_{ex} = 340 nm, λ_{em} = 450 nm) and remaining substrate (λ_{ex} = 340 nm, λ_{em} = 380 nm) was measured, and the ratio of product formed/remaining substrate is reported. Standard curves demonstrate that this fluorescent ratio linearly reflects product under these conditions.

Cell Proliferation Studies. HH and Jurkat cell lines were obtained from ATCC (Manassas, VA, USA) and grown in RPMI 1640 medium supplemented with 10% fetal bovine serum (Gibco, Grand Island, NY, USA). The NIH/3T3 cell line was kindly donated by Dr. Richard Klemke and grown in DMEM medium supplemented with 10% fetal bovine serum (Gibco, Grand Island, NY, USA) at 37 °C in an incubator with 5% CO_2. The CellTiter 96 aqueous one solution cell proliferation assay (MTS) kit was purchased from Promega (Madison, WI, USA). Cell viability was measured using the MTS assay according to the manufacturer's protocol. To start the assay, cells were counted with a hemocytometer, diluted with fresh medium to the proper concentration, and seeded in 96-well plates (5000 cells/well for NIH/3T3 and 20 000 cells/well for HH and Jurkat). Jurkat and HH cells were then directly incubated in media containing the various concentrations of drugs for 70 h (ranging from 0.5 to 128 μM). NIH/3T3 cells were first incubated at 37 °C with 5% CO_2 for 16 h prior to the drug treatment for cell attachment. The cells were then treated with various concentrations of drugs for 70 h. The CellTiter 96 aqueous one solution was added (20 μL per well), and the plate was incubated at 37 °C for 2 h (NIH 3T3) or 4 h (HH and Jurkat). The absorbance was recorded at 490 nm using the BioTek Synergy HT microplate reader. Each concentration of drug treatment was conducted in triplicate for each trail, with 2–3 trials conducted.

Plasma Stability. The plasma stability of SAHA and SAHA-TAP was investigated with pooled normal human plasma (Innovative Research, Novi, MI). In duplicate, plasma (1.0 mL) was preincubated

DOI: 10.1021/acs.jmedchem.5b00539
J. Med. Chem. 2015, 58, 4812–4821

for 2 min at 37 °C followed by the addition of 20 μL of a 5.0 mM stock solution (DMSO). Aliquots (100 μL) were withdrawn at 0, 15, 30, 60, and 120 min and immediately quenched with 100 μL of ACN to precipitate the proteins. The samples were vortexed thoroughly and centrifuged for 2 min at 13 000 rpm. The supernatant was collected and centrifuged through 0.2 μm spin filters (Corning) for 5 min at 8000 rpm. Samples were then frozen until analyzed by HPLC with the following method: analytical HPLC was performed on a HP Series 1050 system equipped with a Poroshell 120 reverse-phase column (EC-C18, 4.6 × 100 mm, 2.7 μm). Separation was achieved with a flow rate of 1 mL min^{-1} and the following mobile phase: 2.5% ACN + 0.1% formic acid in H_2O (A) and 0.1% formic acid in ACN (B). Starting with 95% A and 5% B, a linear gradient was run for 15 min to a final solvent mixture of 5% A and 95% B, which was held for 5 min before ramping back down to 95% A and 5% B over the course of 2 min, with constant holding at this level for 4 additional min.

Western Blot Analysis. Log phase growing HH and Jurkat cell lines were cultured until 70% percent confluent and treated with specified concentrations of compounds for 4 h prior to harvesting. Cells were spun at 250*g* and washed with DPBS buffer (Life Technologies) before lysis using RIPA buffer (50 mM Tris-HCl (pH 7.5), 150 mM Na_2EDTA, 1% Nonidet P-40, 1% sodium deoxycholate, 0.1% sodium dodecyl sulfate) supplemented with complete protease inhibitor cocktail (Roche) for 30 min on ice. Samples were then spun at 12 000*g* before quantification of total protein concentration using a BCA assay (Thermo). Dilutions were made to normalize total protein concentration for each gel sample. Diluted samples were then run on a 10% SDS-PAGE gel at 100 V for 2 h before transfer onto Immobilon-P PVDF Membrane (EMD Millipore) at 100 V for 45 min before blocking in 5% (v/v) Casein-TBST (Tris-buffered saline Tween-20; 0.05% Tween-20 v/v) at 4 °C. Blots were then incubated with monoclonal mouse anti-acetylated tubulin (Life Technologies), polyclonal rabbit anti-tubulin (Sigma), or anti-actin−HRP (Santa Cruz) in 5% (v/v) BSA-TBST at dilutions according to manufacturer's instructions overnight at 4 °C. Blots were then washed by three 5 min washes in TBST (0.05% v/v); anti-acetylated tubulin and anti-tubulin antibodies were then incubated with HRP-conjugated anti-mouse (Santa Cruz) or anti-rabbit (Pierce) antibodies. Detection was performed using SuperSignal West pico substrate (Pierce) with 10% (v/v) SuperSignal West femto substrate (Pierce) and imaged on ChemiDoc XRS+ System with Image Lab Software (Bio-Rad).

■ ASSOCIATED CONTENT

Supporting Information

Synthetic procedures, NMR and MS characterization, analytical HPLC chromatograms, enzyme inhibition assay results, progress curves, and proteomic MS data. The Supporting Information is available free of charge on the ACS Publications website at DOI: 10.1021/acs.jmedchem.5b00539.

■ AUTHOR INFORMATION

Corresponding Authors

*(C.A.F.) E-mail: fierke@umich.edu. Telephone: (734) 936-2678.

*(S.M.C.) E-mail: scohen@ucsd.edu. Telephone: (858) 822-5596.

Author Contributions

K.B.D. conceived the project, synthesized all compounds, and designed and performed experiments. E.D.S. designed experiments, expressed/purified WT HDAC8 and C153A mutant HDAC8, and performed all time-dependent progress curve experiments. Y.C. performed all cell proliferation experiments. J.C.C. performed all western blot experiments. K.B.D., E.D.S., Y.C., J.C.C., P.A.J., C.A.F., and S.M.C. analyzed the data and wrote the manuscript.

Notes

The authors declare no competing financial interest.

■ ACKNOWLEDGMENTS

The authors would like to acknowledge the James E. Bradner laboratory for performing preliminary HDAC inhibition studies and Dr. Majid Ghassemian (UCSD Biomolecular and Proteomics MS Facility) for completing proteomic MS experiments. The authors would also like to thank Drs. David P. Martin and David T. Puerta for helpful discussions. This work was supported by grants from the U.S. National Institutes of Health (NIH) through the National Institute of General Medical Sciences (NIGMS) (R01 GM101467, P.A.J; R01 GM40602, C.A.F.; and R01 GM098435, S.M.C.).

■ ABBREVIATIONS USED

HDAC, histone deacetylase; HDACi, histone deacetylase inhibitor; PK, pharmacokinetics; CTCL, cutaneous T-cell lymphoma; GSH, glutathione in its reduced form; Cys, cysteine

■ REFERENCES

(1) Haberland, M.; Montgomery, R. L.; Olson, E. N. The many roles of histone deacetylases in development and physiology: implications for disease and therapy. *Nat. Rev. Genet.* **2009**, *10*, 32−42.

(2) De Ruijter, A. J. M.; Van Gennip, A. H.; Caron, H. N.; Kemp, S.; Van Kuilenburg, A. B. P. Histone deacetylases (HDACs): characterization of the classical HDAC family. *Biochem. J.* **2003**, *370*, 737−749.

(3) Marks, P. A.; Rifkind, R. A.; Richon, V. M.; Breslow, R.; Miller, T.; Kelly, W. K. Histone deacetylases and cancer: causes and therapies. *Nat. Rev. Cancer* **2001**, *1*, 194−202.

(4) Johnstone, R. W. Histone-deacetylase inhibitors: novel drugs for the treatment of cancer. *Nat. Rev. Drug Discovery* **2002**, *1*, 287−299.

(5) Agalioti, T.; Chen, G.; Thanos, D. Deciphering the transcriptional histone acetylation code for a human gene. *Cell* **2002**, *111*, 381−392.

(6) Matangkasombut, O.; Buratowski, S. Different sensitivities of bromodomain factors 1 and 2 to histone H4 acetylation. *Mol. Cell* **2003**, *11*, 353−363.

(7) Choudhary, C.; Kumar, C.; Gnad, F.; Nielsen, M. L.; Rehman, M.; Walther, T. C.; Olsen, J. V.; Mann, M. Lysine acetylation targets protein complexes and co-regulates major cellular functions. *Science* **2009**, *325*, 834−840.

(8) Gryder, B. E.; Sodji, Q. H.; Oyelere, A. K. Targeted cancer therapy: giving histone deacetylase inhibitors all they need to succeed. *Future Med. Chem.* **2012**, *4*, 505−524.

(9) Dokmanovic, M.; Clarke, C.; Marks, P. A. Histone deacetylase inhibitors: overview and perspectives. *Mol. Cancer Res.* **2007**, *5*, 981−989.

(10) Kantharaj, E.; Jayaraman, R. *Hisone Deacetylase Inhibitors as Therapeutic Agents for Cancer Therapy*; Intech: Rjeka, Croatia, 2011.

(11) Marks, P. A.; Breslow, R. Dimethyl sulfoxide to vorinostat: development of this histone deacetylase inhibitor as an anticancer drug. *Nat. Biotechnol.* **2007**, *25*, 84−90.

(12) *FDA approves Farydak for treatment of multiple myeloma*; U.S. Food and Drug Administration: Silver Spring, MD, 2015. http://www.fda.gov/NewsEvents/Newsroom/PressAnnouncements/ucm435296.htm.

(13) *Belinostat*; U.S. Food and Drug Administration: Silver Spring, MD, 2014. http://www.fda.gov/Drugs/InformationOnDrugs/ApprovedDrugs/ucm403960.htm.

(14) Rubin, E. H.; Agrawal, N. G. B.; Friedman, E. J.; Scott, P.; Mazina, K. E.; Sun, L.; Du, L. H.; Ricker, J. L.; Frankel, S. R.; Gottesdiener, K. M.; Wagner, J. A.; Iwamoto, M. A study to determine the effects of food and multiple dosing on the pharmacokinetics of vorinostat given orally to patients with advanced cancer. *Clin. Cancer Res.* **2006**, *12*, 7039−7045.

DOI: 10.1021/acs.jmedchem.5b00539
J. Med. Chem. 2015, 58, 4812−4821

(15) Flipo, M.; Charton, J.; Hocine, A.; Dassonneville, S.; Deprez, B.; Deprez-Poulain, R. Hydroxamates: relationships between structure and plasma stability. *J. Med. Chem.* **2009**, *52*, 6790−6802.
(16) Andreu-Vieyra, C. V.; Berenson, J. R. The potential of panobinostat as a treatment option in patients with relapsed and refractory multiple myeloma. *Ther. Adv. Hematol.* **2014**, *5*, 197−210.
(17) Rautio, J.; Kumpulainen, H.; Heimbach, T.; Oliyai, R.; Oh, D.; Jarvinen, T.; Savolainen, J. Prodrugs: design and clinical applications. *Nat. Rev. Drug Discovery* **2008**, *7*, 255−270.
(18) Huttunen, K. M.; Raunio, H.; Rautio, J. Prodrugs—from serendipity to rational design. *Pharm. Rev.* **2011**, *63*, 750−771.
(19) Miller, T. A.; Witter, D. J.; Belvedere, S. Patent Application, WO 2005/097747 A1, April 5, 2005.
(20) Schlimme, S.; Hauser, A. T.; Carafa, V.; Heinke, R.; Kannan, S.; Stolfa, D. A.; Cellamare, S.; Carotti, A.; Altucci, L.; Jung, M.; Sippl, W. Carbamate prodrug concept for hydroxamate HDAC inhibitors. *ChemMedChem* **2011**, *6*, 1193−1198.
(21) Estrela, J. M.; Ortega, A.; Obrador, E. Glutathione in cancer biology and therapy. *Crit. Rev. Clin. Lab Sci.* **2006**, *43*, 143−181.
(22) Huang, S. T.; Ting, K. N.; Wang, K. L. Development of a long-wavelength fluorescent probe based on quinone-methide-type reaction to detect physiologically significant thiols. *Anal. Chim. Acta* **2008**, *620*, 120−126.
(23) Thomas, M.; Rivault, F.; Tranoy-Opalinski, I.; Roche, J.; Gesson, J.-P.; Papot, S. Synthesis and biological evaluation of the suberoylanilide hydroxamic acid (SAHA) β-glucuronide and β-galactoside for application in selective prodrug chemotherapy. *Bioorg. Med. Chem. Lett.* **2007**, *17*, 983−986.
(24) Kelly, W. K.; Richon, V. M.; O'Connor, O.; Curley, T.; MacGregor-Curtelli, B.; Tong, W.; Klang, M.; Schwartz, L.; Richardson, S.; Rosa, E.; Drobnjak, M.; Cordon-Cordo, C.; Chiao, J. H.; Rifkind, R.; Marks, P. A.; Scher, H. Phase I clinical trial of histone deacetylase inhibitor: suberoylanilide hydroxamic acid administered intravenously. *Clin. Cancer Res.* **2003**, *9*, 3578−3588.
(25) Furumai, R.; Matsuyama, A.; Kobashi, N.; Lee, K. H.; Nishiyama, N.; Nakajima, I.; Tanaka, A.; Komatsu, Y.; Nishino, N.; Yoshida, M.; Horinouchi, S. FK228 (depsipeptide) as a natural prodrug that inhibits class I histone deacetylases. *Cancer Res.* **2002**, *62*, 4916−4921.
(26) Kim, B.; Pithadia, A. S.; Fierke, C. A. Kinetics and thermodynamics of metal-binding to histone deacetylase 8. *Protein Sci.* **2015**, *24*, 354−65.
(27) McLafferty, F. W. Tandem mass-spectrometry. *Science* **1981**, *214*, 280−287.
(28) Gantt, S. L.; Gattis, S. G.; Fierke, C. A. Catalytic activity and inhibition of human histone deacetylase 8 is dependent on the identity of the active site metal ion. *Biochemistry* **2006**, *45*, 6170−6178.
(29) McClerren, A. L.; Endsley, S.; Bowman, J. L.; Andersen, N. H.; Guan, Z.; Rudolph, J.; Raetz, C. R. A slow, tight-binding inhibitor of the zinc-dependent deacetylase LpxC of lipid A biosynthesis with antibiotic activity comparable to ciprofloxacin. *Biochemistry* **2005**, *44*, 16574−83.
(30) Sculley, M. J.; Morrison, J. F.; Cleland, W. W. Slow-binding inhibition: the general case. *Biochim. Biophys. Acta* **1996**, *1298*, 78−86.
(31) Teitelbaum, A. M.; Meissner, A.; Harding, R. A.; Wong, C. A.; Aldrich, C. C.; Remmel, R. P. Synthesis, pH-dependent, and plasma stability of meropenem prodrugs for potential use against drug-resistant tuberculosis. *Bioorg. Med. Chem.* **2013**, *21*, 5605−5617.
(32) Zhang, C. L.; Richon, V.; Ni, X.; Talpur, R.; Duvic, M. Selective induction of apoptosis by histone deacetylase inhibitor SAHA in cutaneous T-cell lymphoma cells: relevance to mechanism of therapeutic action. *J. Invest. Dermatol.* **2005**, *125*, 1045−1052.
(33) Sodji, Q. H.; Patil, V.; Kornacki, J. R.; Mrksich, M.; Oyelere, A. K. Synthesis and structure−activity relationship of 3-hydroxypyridine-2-thione-based histone deacetylase inhibitors. *J. Med. Chem.* **2013**, *56*, 9969−9981.
(34) Zhang, Y.; Li, N.; Caron, C.; Matthias, G.; Hess, D.; Khochbin, S.; Matthias, P. HDAC-6 interacts with and deacetylates tubulin and microtubules in vivo. *EMBO J.* **2003**, *22*, 1168−79.
(35) Bantscheff, M.; Hopf, C.; Savitski, M. M.; Dittmann, A.; Grandi, P.; Michon, A. M.; Schlegl, J.; Abraham, Y.; Becher, I.; Bergamini, G.; Boesche, M.; Delling, M.; Dumpelfeld, B.; Eberhard, D.; Huthmacher, C.; Mathieson, T.; Poeckel, D.; Reader, V.; Strunk, K.; Sweetman, G.; Kruse, U.; Neubauer, G.; Ramsden, N. G.; Drewes, G. Chemoproteomics profiling of HDAC inhibitors reveals selective targeting of HDAC complexes. *Nat. Biotechnol.* **2011**, *29*, 255−65.
(36) Gryder, B. E.; Akbashev, M. J.; Rood, M. K.; Raftery, E. D.; Meyers, W. M.; Dillard, P.; Khan, S.; Oyelere, A. K. Selectively targeting prostate cancer with antiandrogen equipped histone deacetylase inhibitors. *ACS Chem. Biol.* **2013**, *8*, 2550−60.

DOI: 10.1021/acs.jmedchem.5b00539
J. Med. Chem. 2015, 58, 4812−4821